International Journal of Computational Methods and Experimental Measurements
Vol. 13, No. 2, June, 2025, pp. 239-249
Journal homepage: http://iieta.org/journals/ijcmem

Development and Evaluation of Physically Based Fatigue Damage Model in Textile-Reinforced Plastics

Auday S. Hadi[1], Mohammed M. Azzawi[2], Atheer R. Abdullah[2*]

[1] Mechanical Engineering Department, University of Technology- Iraq, Baghdad 10066, Iraq
[2] Department of Refrigeration and Air Conditioning, Al-Rafidain University College, Baghdad 10001, Iraq

Corresponding Author Email: atheer_raheem@ruc.edu.iq

https://doi.org/10.18280/ijcmem.130203

Received: 21 December 2024
Revised: 15 May 2025
Accepted: 21 May 2025
Available online: 30 June 2025

Keywords:
cyclic loading behavior, damage evolution, fatigue numerical modeling, fibre-plastic composites, multilayer composites, textile-reinforced plastics

ABSTRACT

Fiber-plastic composites are increasingly used in the aerospace, automotive, and wind energy industries, often exposed to multi-axial mechanical loads and high climatic stresses. The objective of this study is to investigate the fatigue behavior of these composites as a function of multi-axial mechanical stress by a novel developed degradation model based on continuum-damage-mechanical approaches. The model's simulation performance has been examined and demonstrated it is applicable in engineering practice. CFRC composites exhibit 74.5 MPa of tensile strength, but GF(MLG)/EP glass fiber reinforced composites demonstrate a considerable lack in both stiffness and regular deformation until ultimate failure. The failure of textile-reinforced plastic composites occurred in three stages of degradation. The tensile strength of biaxial NCF glass-reinforced polyester material was increased by 13 percent as well as the fatigue endurance by 20 percent as compared to the woven roving reinforced composites. The damage onset was 25-35% of the beginning stage. The structure then stabilized to 10-15% and then failed. In GF-MLG/EP, a pattern of stiffness change according to a direction was observed, where transverse cracks reduced the stiffness to 75% of its initial value after 10,000 cycles. Fatigue damage is more resistant in biaxial NCF composites than in woven fabric composites.

1. INTRODUCTION

Predetermination of material mechanical behavior under mechanical, thermal, and loads is crucial for optimal utilization of lightweight construction potentials in technical structures, including static, cyclic, and dynamic components made from conventional and multi-component materials [1]. New material classes like fiber-reinforced plastics are expected to drive development, with textile reinforcement structures preferred due to their high placement variability, automation, and good mechanical characteristics.

However, 3D textile reinforcements with stretched thread arrangement, such as 3D fabrics, multilayer knitted, and warp-knitted fabrics, offer excellent rigidity, strength, resistance to delamination, and good durability. Recent advancements in the material-mechanical behavior of textile-reinforced plastics under quasi-static loads have improved, but there is limited scientific knowledge about fatigue behavior and modeling in-depth experience. The current design relies on cyclic loads, insufficient material degradation, and stress redistribution mapping. Experimental studies show that textile-reinforced plastic components can offer large load-bearing reserves, even with large cracking areas. New, physically based degradation models can significantly improve conventional design methods. This study examines the damage and failure behavior of textile-reinforced multilayer composites under cyclic mechanical loading, aiming to verify the service life of lightweight structures in fiber composite construction. A layer-related degradation model for analyzing damage behavior in GF-MLG reinforced plastics using phenomenological methods was developed. The study emphasizes layer-by-layer and direction-dependent damage descriptions in textile-reinforced plastics, considering structural design variety and cyclic loading [2]. Characterization and modeling of deformation and failure behavior are complex due to heterogeneous material structure. Static loading in classic plastic composites has led to the development of elasticity theory and failure and damage models for describing first-layer failure and successive degradation behavior [3-5]. Material behavior in fiber-reinforced composites requires distinction between individual layers, multilayer composites, and textile-reinforced composites [6].

Stress-strain behavior of a unidirectional fiber-reinforced single layer with a plastic matrix is brittle, with damage causing fiber and inter-fibre fractures, leading to layer failure. Multilayer multi-axial connected composites can divert or stop cracks in damaged layers when they reach neighboring layers, despite brittle fracture behavior at micro and meso levels. Mathematical descriptions of material behavior under quasi-static stress are available [7]. The crack-stopping effect is enhanced when the fabric is combined with textile

reinforcement architecture, fiber undulation, and sewing or knitting threads [8]. The damage phenomenology, particularly in reinforcements with strong fiber undulation, is primarily due to diffuse damage, which requires quantification without justifiable experimental stress [9-11]. Dobrzański [11] suggests that layer-related modeling of textile-reinforced plastics with static loads beyond the elastic range can be achieved through targeted observation and measurement. Recent work explores the elastic and pseudo-plastic behavior of textile-reinforced plastics using physical and cross-scale damage-mechanical approaches, modeling and realistically predicting multiple cracking in multilayers [12, 13]. Scientific understanding of fiber and textile-reinforced plastics' damage behavior due to cyclic loads is limited, with brittle failure and large fatigue strength scatter influencing lifetime [14].

Multilayer composites, like static loads, experience crack deflection effects, resulting in pseudo-plastic material behavior [15, 16]. Matrix transverse cracks in vertical fiber layers cause interface failure and crack growth, leading to delamination and damage. Multilayer laminates characterize this fatigue behavior. Multiple cracking causes a drop in stiffness in the load direction, with degrading stiffness dropping into three areas: digressive, linear, and progressive [17, 18]. The formation of multiple cracks in different fracture modes results in stress redistribution from damaged to undamaged layers.

Rezasefat et al. [19] used Cuntze's failure mode concept to analyze stress in GF-MLG/EP, identifying five independent fracture modes for planar stresses. They identified two fiber fracture modes (FF4 1 and FF 2) and three fracture modes (IFF5 1 to 3) for inter-fibre breakage under tensile, compressive, and shear stress. The degradation of direction-dependent stiffness parameters, such as transverse cracks in [0/90] laminates subjected to tension pulsations, leads to a decrease in stiffness in the direction of tension. Wharmby's research focuses on the impact of various damage phenomena on the stiffness behavior of reinforced materials, as detailed by Zhang et al. [20]. Textile reinforcement materials with fiber undulation exhibit more pronounced damage behavior under complex loads under cyclic loads, with a higher proportion of diffuse damage compared to unidirectional monolayer composites [21, 22].

The fatigue strength of UD-reinforced layers with in-phase multi-axial loading can be determined using physical failure calculation criteria.

The damage evolution of glass fiber-reinforced duromers and carbon fiber-reinforced plastics can be quantified using in-situ light microscopy and crack density measurements, along with high-resolution computed tomography [8]. Their test results show that glass fiber-reinforced composites experience a significant drop in stiffness due to material Damage, while carbon fiber-reinforced plastics only experience a slight decrease by the end of their service life.

The stiffness of multilayer or textile-reinforced plastic composites decreases in stages, starting digressive, linear up to 80%, and progressing towards the end of life. Fiber-reinforced plastics have superior fatigue properties compared to conventional materials [23]. Adam et al. [24] suggest that analyzing and modeling fiber-reinforced plastics under cyclic loading requires considering specific influences, like medium stress, based on static load experiences.

Lightweight construction, particularly textile-reinforced plastics, plays a crucial role. However, knowledge of material-mechanical behavior and fatigue behavior remains limited, making the use of high-performance materials in air, aerospace, and vehicle construction a major challenge. This work develops a mathematical model that is able to evaluate the damage due to stress cycles in the material under cyclic loading. The paper discusses the development of physical damage for textile-reinforced materials, specifically plastics, subjected to cyclic stress. It suggests reducing the damaging effect of complex cyclic stresses to increase material utilization. The model includes damage phenomenology, multi-axial loading, and numerical investigations.

2. MATERIALS AND METHODS

Numerous model approaches describe the degradation of characteristic value and service life of fiber-reinforced plastics under cyclic loading. To model these composites, material-mechanical modeling at base layers and phenomenological cross-scale strategies are beneficial. The damage model developed by Philippi is an extension of the Vassilopoulos model, which uses linear damage accumulation for single and multilayer fibrous reinforced plastics. Failure conditions for orthotropic failure composite materials with in-phase cyclic-harmonic stress, using S-N curves for pulsating tensile, compressive, and shear stresses provided. They propose using Goodman diagrams for deviating stress ratios. Extensive experimental results show good prediction accuracy for fiber-reinforced plastics. Stress concentration in laminated composites reduces fatigue life, increasing at high cycles. Stress concentration factor (1-3) correlates fatigue strength between sharp and round-edge GFRP composites [25]. The Miner rule extends the general damage model, enabling service life prediction under operating stresses. Accuracy depends on material sensitivity and load sequence effects, as a chronological sequence of cyclic loads is lost.

The macro-level criterion for new S-N curves requires constant determination of layer structure changes, and computational optimization of composite material service life and residual stiffness capacity and strength is not possible.

The study uses a continuum-damage-mechanical approach to mathematically describe the degradation of textile-reinforced plastics under cyclic loading, focusing on direction-dependent damage parameters and fractional mode-related stress.

Table 1. Material properties of GF-MLG/EP composite

Property	Value	Test Standard
Fiber Volume Fraction	33%	ASTM D3171
Matrix Material	Epoxy Resin	-
Density (g/cm³)	1.85	ASTM D792
Tensile Strength (MPa)	450	ASTM D3039
Young's Modulus (GPa)	23	ASTM D3039
Shear Strength (MPa)	80	ASTM D5379
Fatigue Strength (MPa, 10^6 cycles)	150	ASTM D3479

2.1 Materials and their properties

When studied as a material for applications in aerospace and automotive industries, a multiple-layer grid reinforcement system is found in the glass fiber existing in epoxy (EP) resin. Mechanical characteristics thus verified were found in accordance with manufacturer-specified values, as shown in Table 1.

Vacuum-assisted resin infusion molding (VARIM) was used to create the composite mathematical model development. Fatigue behavior of these composites as a function of multi-axial mechanical stress by a novel developed degradation model based on continuum-damage-mechanical approaches.

2.2 Development of degradation model

For applications in aerospace and automotive industries, a multiple-layer grid reinforcement system is found in the glass fiber existing in epoxy (EP) resin. Mechanical characteristics thus verified were found in accordance with manufacturer specified values. To describe the incremental directional growth of the damage at the mesoscopic level, damage evolution equations are chosen, which, as a sum of the damage increments assigned to the fracture modes, are formulated. The fracture mode-related damage increment functions are a function of the respective material. This means that the current load step also contains information about the completed load history. An incremental formulation of the evolution equation is used to capture the load history.

The study uses damage evolution equations to describe the incremental growth of damage at the mesoscopic level, focusing on fracture modes and their related increment functions. The proven coupling of the damage occurs at the model level through the introduction of coupling factors qi∗, with the help of fracture mode-related damage increment functions of different fracture modes coupled with the damage parameters Di (i = 1, 2, 6). The model-level coupling of damage occurs through coupling factors and fracture mode-related increment functions.

$$\frac{dD_i}{dn} = \varphi^* q_i^* \ (*= \|\sigma, \|T, \perp \sigma, \perp T, \perp\|)^6 \tag{1}$$

Eq. (1) represents the evolution of the damage parameter D_i with respect to the number of cycles n, involving damage growth functions, φ^* and q_i, parameters. The equation also includes terms involving stresses σ and T, possibly representing material stresses and shear stresses, with the superscripts denoting perpendicular components.

Conventional lifetime models do not consider load cycles. Instead, they focus on material condition and current stress, as shown in Eq. (1) for plane stress state.

$$\frac{dD_i}{dn} = \frac{d}{dn}\begin{bmatrix} D_1 \\ D_2 \\ D_6 \end{bmatrix} = \left(\varphi^{\|\sigma}\begin{bmatrix} q_1^{\|\sigma} \\ q_2^{\|\sigma} \\ q_6^{\|\sigma} \end{bmatrix}\right) + \left(\varphi^{\|T}\begin{bmatrix} q_1^{\|T} \\ q_2^{\|T} \\ q_6^{\|T} \end{bmatrix}\right) + \left(\varphi^{\perp\sigma}\begin{bmatrix} q_1^{\perp\sigma} \\ q_2^{\perp\sigma} \\ q_6^{\perp\sigma} \end{bmatrix}\right) + \left(\varphi^{\perp T}\begin{bmatrix} q_1^{\perp T} \\ q_2^{\perp T} \\ q_6^{\perp T} \end{bmatrix}\right) + \left(\varphi^{\perp\|}\begin{bmatrix} q_1^{\perp\|} \\ q_2^{\perp\|} \\ q_6^{\perp\|} \end{bmatrix}\right) \tag{2}$$

Eq. (2) describes the evolution of the damage parameter D_i. With respect to the number of cycles n, using a series of terms based on various stress and strain components, including both parallel and perpendicular components of stress (σ) and shear stress (T). Each term involves a function φ and various coupling parameters denoted by q, associated with the different orientations (parallel and perpendicular) of the stresses.

The mathematical formulation of damage growth functions φ∗ is based on the determined layer-related crack density increase, with criteria including realistic material degradation, minimal model parameters, and simple equation manageability.

Suggested that a constant, such as scaled fracture mode-related material stress, is available for continuously increasing damage as a damage growth function.

$$\varphi(D, F) = \varphi(F) = c.F \tag{3}$$

This equation suggests a linear relationship between the function φ, the damage parameter D, and the force F. The function φ appears to be directly proportional to the force F, with c being the proportionality being constant.

The model of material stress's influence on fatigue strength behavior can be enhanced by replacing stress *F* in Eq. (3) with power or exponential functions of stress.

$$\varphi(F) = c_1 F^{c2} \tag{4a}$$

$$\varphi(F) = c_1 e^{c2.F} \tag{4b}$$

Eqs. 4(a) and 4(b) describe the function φ in terms of the force F, using different functional forms. The first equation represents a power law relationship where c_1 and c_2 are constants, and the force F is raised to the power c_2. The second equation represents an exponential relationship, where the force F is multiplied by a constant c_2, and the exponential function governs the behavior.

The damage increases linearly with load cycles, determined by reaching the maximum stress or critical damage Dc in the calculation cycle, indicating a direction-dependent damage state.

Eq. (4) is utilized to effectively depict the numerically determined increase in Damage of GFMLG/EP composites in the case of plane shear stress and tensile stress parallel to the fibers.

It was found that in addition to linear damage progression, digressive damage increases were also observed in phenomenological considerations.

$$\varphi(D, F) = c_1 F(D_s - D) \tag{5}$$

This equation represents a function φ that depends on both the damage parameter, *D,* and the force, *F*. Here, c_1 is a constant, *Ds* is a reference or saturation damage value, and *D* is the current damage level. The equation suggests that the function φ is proportional to the force *F* and the difference between the saturation damage, D_s, and the current damage, *D*. This form is likely used to model how the damage parameter evolves as the material undergoes loading.

$$\varphi = c_1 F e^{(-c2\frac{D}{\sqrt{F}})} \tag{6}$$

Such damage growth functions with a digressive progression are used within the framework of this work to describe the damage in fracture mode IFF1. For fracture modes with sudden-death damage characteristics, the use of a damage growth function is proposed by Dean et al. [5]:

$$\varphi(D, F) = c_1.D.F\left(1 + e^{c_2(F - c_3)}\right) \tag{7}$$

The selection of suitable damage increment functions from Eqs. (1) to (7) takes place on a material-specific basis using

the numerically determined drop in stiffness.

Damage increment functions based on Eqs. (6) and (7) can be influenced by model parameters (D > 1) or invalid values, necessitating a termination criterion for practical application cases.

Damage growth functions describe the evolution of damage in fracture modes, affecting direction-dependent stiffness degradation based on geometrical characteristics and coupling vectors.

The numerically determined coupling parameter , $q_6^{||\sigma}$, determines the increase in damage $\varphi^{||\sigma}$ due to shear stress degradation, with negligible influence on damage perpendicular to the grain direction.

$$q_i^{||\sigma} = \begin{bmatrix} 1 \\ 0 \\ q_6^{||\sigma} \end{bmatrix} \tag{8}$$

This equation represents a vector notation for $q_i^{\|\sigma}$, where: $q_i^{\|\sigma}$ is a vector associated with the stress components in the direction of the fibers ($\|\sigma$).

The first element of the vector is 1, and the second element is 0. The third element is $q_6^{\|\sigma}$, which is another component of the damage model, likely representing some form of coupling or interaction in the stress direction.

This structure likely appears in the context of a more complex system modeling the behavior of materials under cyclic loading or stress, where the vector components represent different damage parameters for various failure modes or orientations.

Damage in IFF1 fracture mode does not affect fiber degradation direction, while Damage in IFF2 fracture mode influences the coupling parameter, $q_1^{\perp||}$. In addition, the coupling between IFF2 and the degradation transverse to the grain direction via $q_2^{\perp||}$, the influence of damage in fracture mode IFF1 with the coupling parameter $q_6^{\perp\sigma}$ on the characteristic values for shear stress. The associated coupling vectors $q_i^{\perp\sigma}$ and $q_i^{\perp||}$ result in:

$$q_i^{\perp\sigma} = \begin{bmatrix} 0 \\ 1 \\ q_6^{\perp\sigma} \end{bmatrix} \text{and } q_i^{\perp||} = \begin{bmatrix} q_1^{\perp||} \\ q_2^{\perp||} \\ 1 \end{bmatrix} \tag{9}$$

These equations describe two vectors related to the damage parameters in the material model:

$q_i^{\perp\sigma}$: This is a vector associated with stress components that are perpendicular to the fiber direction ($\perp \sigma$), where:

The first component is 0.

The second component is 1.

The third component is $q_6^{\perp\sigma}$, a damage parameter specific to the perpendicular stress components.

$q_i^{\perp\perp}$: This vector is associated with damaged components in the perpendicular direction of both stress and strain ($\perp\perp$), where:

The first component is $q_1^{\perp\perp}$, a parameter for the first perpendicular componet.

The second component is $q_2^{\perp\perp}$, another perpendicular parameter.

The third component is 1.

These vectors are used to describe the interaction between different stress and strain components, particularly in modeling how damage progresses in different material directions under loading conditions.

In the case of damage initiation in fracture mode, FF2 and IFF3 are total failures of the association. The vectors $q_6^{\perp\tau}$ and $q_i^{\perp\tau}$ are, therefore, without restriction, to set the general public according to:

$$q_i^{||\tau} = \begin{bmatrix} 1 \\ 1 \\ 1 \end{bmatrix} q_i^{\perp\tau} = \begin{bmatrix} 1 \\ 1 \\ 1 \end{bmatrix} \tag{10}$$

These two equations describe vectors associated with the shear stress components, τ:

- $q_i^{\|\tau}$: This vector is related to shear stress components in the direction of the fibers ($\|\tau$), where all components are equal to 1.
- $q_i^{\perp\tau}$: This vector is related to shear stress components in the perpendicular direction to the fibers ($\perp \tau$), where all components are also equal to 1.

Both vectors are used to model how damage or other material properties change under shear stress in different orientations, specifically along and perpendicular to the fiber direction. The yet undetermined coupling parameters are determined using the directional and load-type dependent stiffness degradation with multi-axial loading and can also assume values above one.

2.3 Damage model evolution

The study evaluates the stiffness degradation of [0/90] composites in uniaxial cyclic tests for each fracture mode, focusing on layer-specific damage phenomenology, even with uniaxial external load. The damage increment functions $\varphi^{||\sigma}$ and $\varphi^{\perp\sigma}$ of the fracture modes IFF1 and FF1 is determined with the help of the stiffness degradation of the [0/90] composite with uniaxial tensile pulsating loading. The initial phase I of tensile pulsating load results in a digressive decrease in rigidity, primarily resulting in transverse cracks in the perpendicular layer, with minimal damage increase. For the base layers (index: 90° and 0°) during the first phase of the drop in stiffness, the damage evolution equation simplifies to,

$$\begin{aligned} \frac{\mathrm{d}}{\mathrm{d}n}\begin{bmatrix} D_1 \\ D_2 \\ D_6 \end{bmatrix}\Bigg|_{90^\circ} &= \left(\varphi^{\perp\sigma} \begin{bmatrix} q_1^{\perp\sigma} \\ q_2^{\perp\sigma} \\ q_6^{\perp\sigma} \end{bmatrix} \right) \neq 0 \\ \frac{\mathrm{d}}{\mathrm{d}n}\begin{bmatrix} D_1 \\ D_2 \\ D_6 \end{bmatrix}\Bigg|_{0^\circ} &= \left(\varphi^{||\sigma} \begin{bmatrix} q_1^{||\sigma} \\ q_2^{||\sigma} \\ q_6^{||\sigma} \end{bmatrix} \right) = 0 \end{aligned} \tag{11}$$

The coupling vectors become general without restriction:

$$q_i^{||\sigma} = \begin{bmatrix} 1 \\ 0 \\ 0 \end{bmatrix}, \text{ and } q_i^{\perp\sigma} = \begin{bmatrix} 0 \\ 1 \\ 0 \end{bmatrix} \tag{12}$$

These equations describe the damage evolution during Phase I of the material's degradation process.

The first equation represents the damage evolution at 90° orientation, where the damage parameters D_1, D_2 , and D_6 evolve based on the applied stress and coupling vectors (represented by $q_1^{\|\sigma}, q_2^{\|\sigma}$, and $q_6^{\|\sigma}$) under a non-zero damage rate.

The second equation represents the evolution of the damage parameters at 0° orientation, where the same stress components drive the damage evolutions but result in a zero rate of change, suggesting no further damage progression under these conditions. This suggests that Phase I involves a stage where the material undergoes some damage under specific conditions but stabilizes under certain orientations.

For the degradation and fatigue strength behavior of stress-related in the case of ionized fiber composite components, the damage behavior in the direction of the fibers is still the decisive factor. The associated damage increment function $\varphi^{||\sigma}$ is determined to correspond to the small linear drop in stiffness in phase II. The damage evolution equation simplifies to:

$$\begin{aligned} \frac{\mathrm{d}}{\mathrm{d}n}\begin{bmatrix} D_1 \\ D_2 \\ D_6 \end{bmatrix}\Bigg|_{90^\circ} &= \left(\varphi^{\perp\sigma}\begin{bmatrix} q_1^{\perp\sigma} \\ q_2^{\perp\sigma} \\ q_6^{\perp\sigma} \end{bmatrix}\right) = 0, \\ \frac{\mathrm{d}}{\mathrm{d}n}\begin{bmatrix} D_1 \\ D_2 \\ D_6 \end{bmatrix}\Bigg|_{0^\circ} &= \left(\varphi^{||\sigma}\begin{bmatrix} q_1^{||\sigma} \\ q_2^{||\sigma} \\ q_6^{||\sigma} \end{bmatrix}\right) \neq 0 \end{aligned} \tag{13}$$

These equations describe the material behavior during Phase II:

The first equation represents the evolution of the damage parameters at 90° orientation, where the damage evolution rate is zero. This suggests that during Phase II at this orientation, no further damage progression occurs, implying stabilization.

The second equation shows that at the 0° orientation, the damage evolution is non-zero, indicating ongoing damage progression under these conditions. This phase indicates a transition in the material's behavior where damage might stop under certain conditions at 90° but continues in others at 0°.

The damage evolution equation can be simplified by assuming identical properties of the two idealized base layers uniform to:

$$\frac{\mathrm{d}}{\mathrm{d}n}\begin{bmatrix} D_1 \\ D_2 \\ D_6 \end{bmatrix}\Bigg|_{0^\circ,90^\circ} = \left(\varphi^{\perp||}\begin{bmatrix} q_1^{\perp||} \\ q_2^{\perp||} \\ q_6^{\perp||} \end{bmatrix}\right) \neq 0,$$

with

$$q_i^{\perp||} = \begin{bmatrix} 0 \\ 0 \\ 1 \end{bmatrix} \tag{14}$$

In Eq. (4):

- The rate of change of the damage parameters D_1, D_2, and D_6 are calculated for a material under loading conditions at both 0° and 90° orientations.
- The function $\varphi^{\perp\perp}$ governs the damage evolution in the perpendicular direction for stress and strain.
- The vector $q_i^{\perp\perp}$ is given, with specific components for the perpendicular direction, where the last element is 1, and the first two are 0.

This indicates a condition where the damage evolution is influenced by the perpendicular components of stress/strain and is non-zero. It implies that material damage is progressing under these conditions. The variations key for identifying suitable damage models are summarized in Table 2.

Table 2. Variations key for identifying suitable damage models

Figure	Model Type	Equation	Key Effect
(a)	Linear (Damage Constant c)	$\phi(F) = c \cdot F$	Higher c increases damage linearly.
(b)	Linear (Force F)	$\phi(F) = c \cdot F$	Higher FF increases damage linearly.
(c)	Exponential Model	$\phi(F) = c_1 e^{c_2 F}$	Damage accelerates non-linearly, leading to sudden failure.
(d)	Power-Law Model	$\phi(F) = c_1 F^{c_2}$	Damage increases gradually, and more stable failure.

The present variations are key for identifying suitable damage models for textile-reinforced composites under cyclic loading. However, careful calibration of the parameters is indicated to properly predict the products' lifetimes.

3. RESULTS AND DISCUSSION

3.1 Influence of the parameter selection

The constant stress during cyclic loading leads to a linear increase in damage over the number of load cycles, as shown in Figure 1. Figures of the dependence of D on real lifetime under cyclic loading conditions demonstrate the dependence upon parameter selection when the constant increase is observed. Real lifetime curves are plotted against damage evolution for different parameter values to show the variation of the degradation behavior under various stress conditions.

The progression of damage as c is varied ($\phi(F) = c \cdot F$). Figure 1(a) shows the relationship between Damage (D) and real lifetime when the damage growth constant (c) is varied under a constant force of F = 0.5. The values of 0.00016, 0.00014, 0.00012, and 0.0001 represent four curves and a different value of growth constant, c. The damage evolution function is linear, which means that the damage increases linearly with time, and the trend appears to indicate that c leads to damage increasing faster over time.

Figure 1(b) shows the influence of force F ($\phi(F) = c \cdot F$) on damage evolution. The effect of the changing force levels (F = 0.2, 0.3, 0.4, 0.5) on damage progression is illustrated in this figure. For the damage growth constant c = $0.4E^{-4}$ and the number of cycles N = 10,000, they are fixed. The greater squeeze force levels more quickly promote damage development. That is, increasing the applied loads changes the rates of material degradation. It is found that the linear trend implies a proportional relationship between damage accumulation and force.

Figure 1(c) shows the function's impact on the growth of damage. In this case, the damage evolution is not a straightforward linear relationship but an exponential model. The function which is used is $\phi(F) = c_1 e^{c_2 F}$ and c_1=0.4E−5 and c_2=10. The damage increases much steeper exponentially (F = 0.1, 0.2, 0.3, 0.4) than in linear models and suggests that some materials may exhibit nonlinear damage buildup with increasing load amplitudes leading to early failure.

Figure 1(d) shows the power-law function's impact on the evolution of damage. This graph uses a power-law function to depict the growth of damage: $\phi(F) = c_1 F^{c_2}$. The parameters are as follows: c_1 = $1.4E^{-4}$, and c_2 = 0.5. Once more, the force readings (F = 0.1, 0.2, 0.3, 0.4) show growing damage. This

function exhibits a slightly curved trajectory in contrast to the linear (a, b) and exponential (c) models, suggesting a nonlinear but less aggressive damage increase than (c).

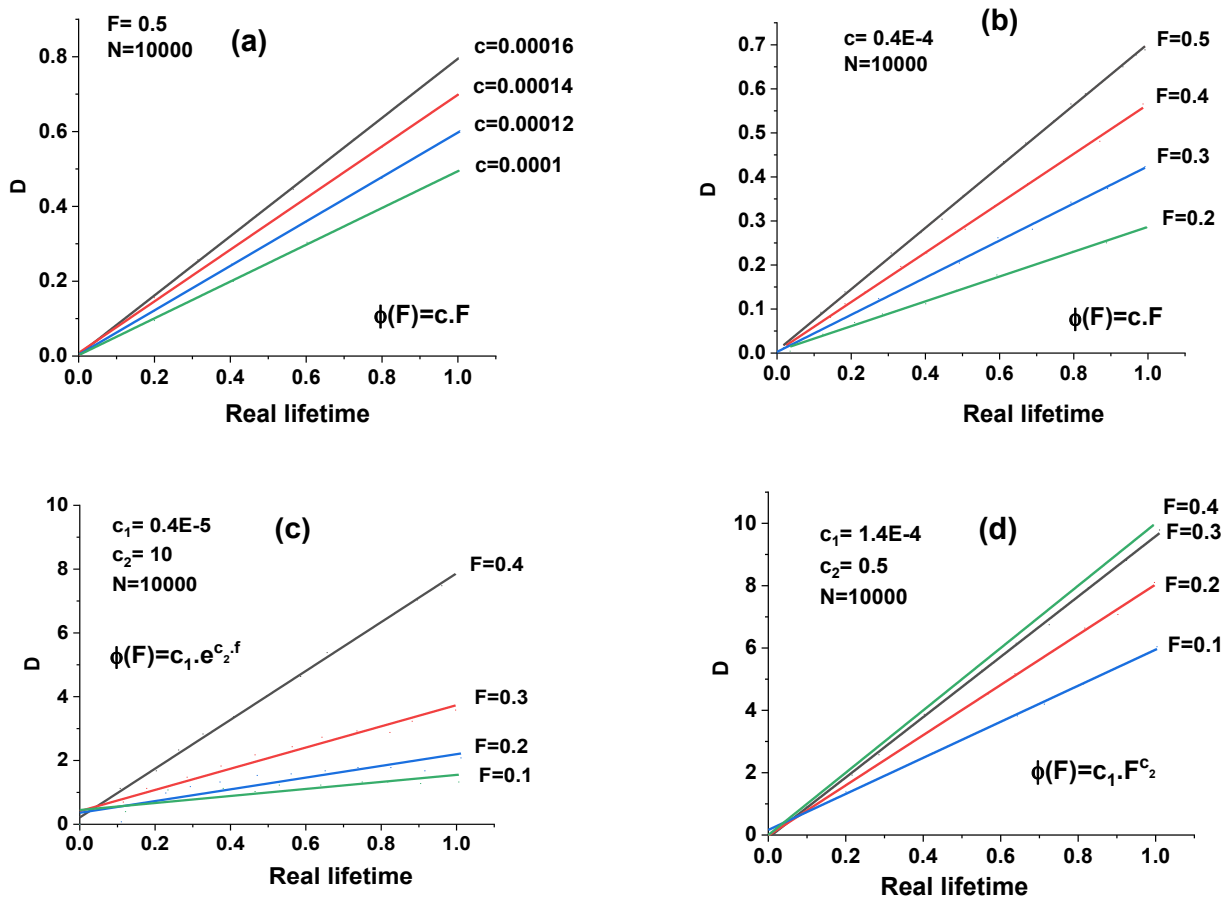

Figure 1. Influence of the damage parameter (D) selection for the constant increase in damage according to Eqs. (1 to 3)

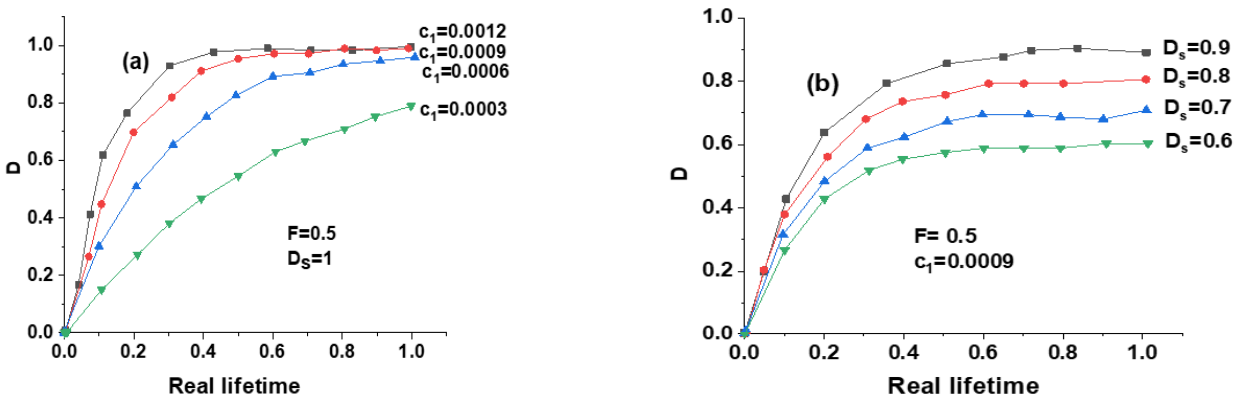

Figure 2. Influence of the material parameters c_1 and Ds on the course of the damage parameter D according to Eq. (5)

The material stress, F, damage parameter, D, and saturation limit, Ds with $0 \leq Ds \leq 1$, are related to the residual load-bearing capacity of embedded damaged layers, with Ds indicating shear stress bridging and c_1 indicating strong damage growth at load map start (see Figure 2).

Figures 2(a) and 2(b) illustrate the influence of material parameters c_1 and Ds on the evolution of the damage parameter D over time.

Figure 3(a) shows the influence of the material parameter, c_1, on the damage parameter D, with a constant D_s = 1 and force F = 0.5. The graph plots D as a function of the real lifetime for different values of c_1, which represents how the material parameter affects damage evolution over time.

Figure 3(b) shows the influence of the material parameter, c_2, on the damage parameter D, with a constant $c_1 = 0.0009$ and force F = 0.5. The graph plots D as a function of the real lifetime for different values of D_s, which represents how the saturation damage level D_s affects damage evolution over time. A characteristic comparable to the saturation function has exponential functions of the type [25].

An impact of model parameters c_1, c_2, c_3 and applied stress F on damage parameter D over a material lifetime is seen in Figure 4(a-d). Equation (7) includes exponential as well as linear damage growth components. For the higher values of c_1 the damage accumulation is faster, and for lower values, slower. After ~ 0.7 of real lifetime, the damage parameter D increases sharply, indicating an accelerated failure mechanism. Values of c_2 with larger values correspond to a steeper increase of damage near failure and smaller values with a lower value of damage close to failure. This indicates that exponential damage effects are dominant in the last failure phase. The threshold for damage initiation is regulated by c_3, and the damage initiation starts accumulating significantly only above that threshold. A steeper rise occurs at higher values of c_3; a steeper but delayed rise occurs if values of c_3 are lower. It can be seen in this graph that damage accumulation proceeds faster for greater stress levels, and the material lifetime is lower. For F = 0.55, the damage is 100% at much earlier than real lifetime = 1.0, while lower stress levels yield the slower, more gradual damage accumulation. The combination of high c_1, c_2, and F results in catastrophic failure early in the lifetime. Higher F and c_1 result in a more sudden damage accumulation and, hence, shorter service life.

The figure presents four graphs showing the influence of material parameters. c_1, c_2, and c_3, as well as stress F, on the damage parameter D according to Eq. (7). The graphs are labeled as (a), (b), (c), and (d), each highlighting different aspects of the parameter variations:

- Figure 4(a): Shows the influence of varying c_1, where $c_2 = 5, c_3 = 6 \times 10^{-6}$, and $F = 0.5$.
- Figure 4(b): It shows the influence of varying c_2, where $c_3 = 6 \times 10^{-6}$, and $F = 0.5$.
- Figure 4(c): It shows the influence of varying c_3, where $c_2 = 5$, and $F = 0.5$.
- Figure 4(d): It shows the influence of varying F, where $c_2 = 5, c_3 = 6 \times 10^{-6}$.

These graphs illustrate how the damage parameter changes as different material parameters and stress levels are varied, according to the model described by Eq. (7).

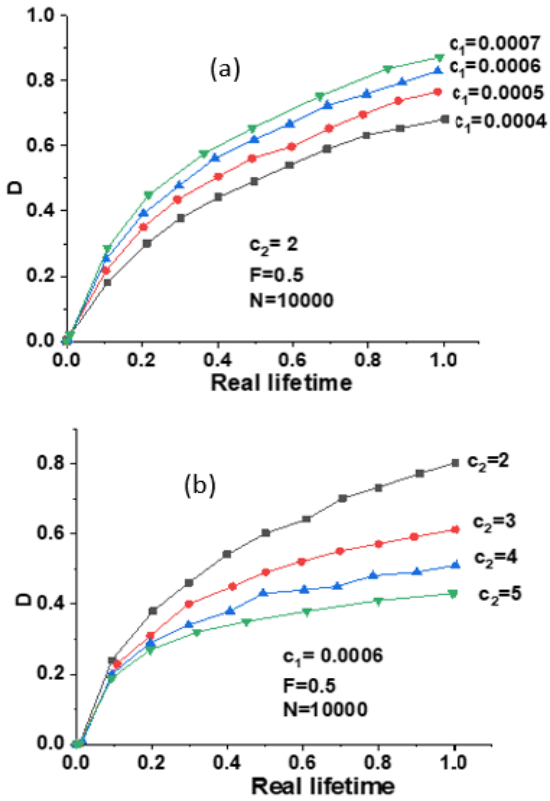

Figure 3. Influence of the material parameters: (a) c_1 and (b) c_2 on the course of the damage parameter D according to Eq. (6)

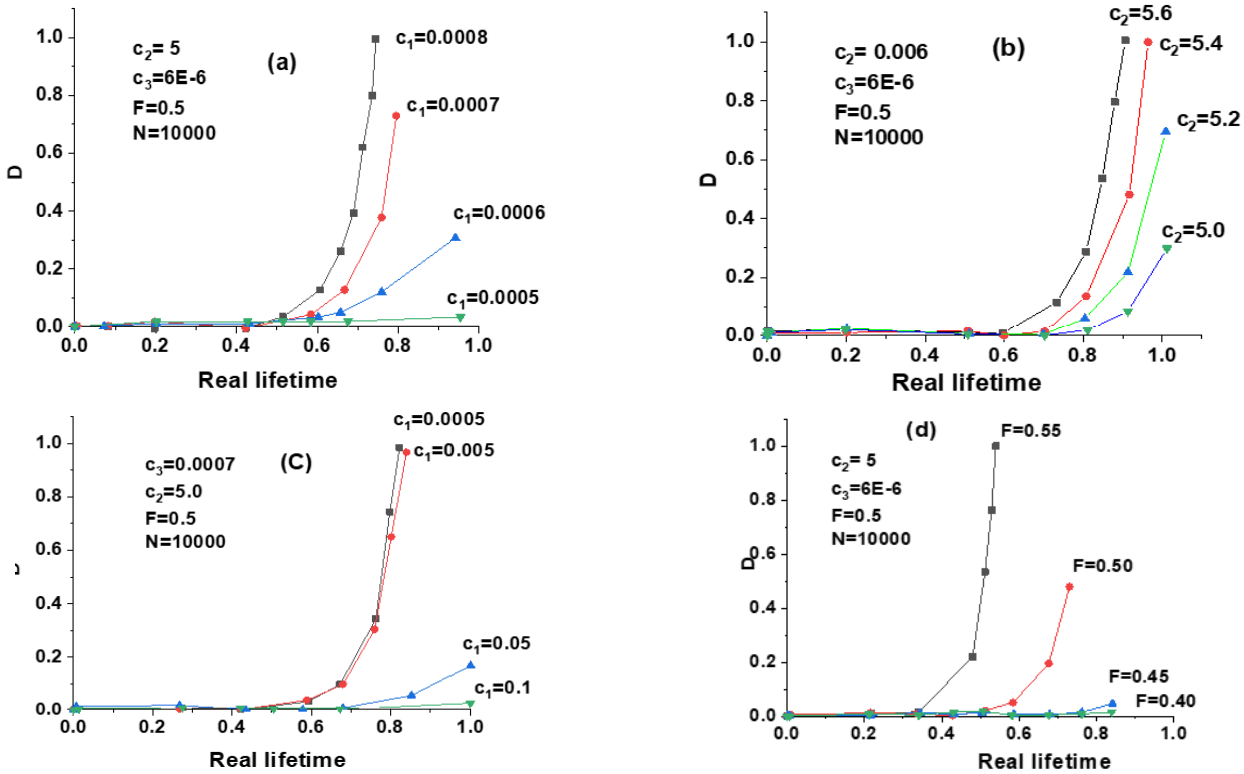

Figure 4. Influence of the material parameters c_1, c_2, and c_3 and the stress F on the course of the damage parameter D according to Eq. (7)

3.2 Parameter identification

For the identification of the model parameters of the damage initiation, V_w and N_w, the damage evolution, c_i, D_s, and D_c, the coupling vectors, q, as well as the influencing parameters of the passive damage, h_i, the results of the uniaxial and multi-axial fatigue strength tests described in the Literature available data are used. In addition to the fatigue strength diagram in particular, the stiffness curves ($E_{dyn}(N)$ and $G_{dyn}(N)$) are evaluated. It was found that biaxial NCF glass-reinforced polyester, with a volume fraction of 33%, has superior mechanical properties compared to woven roving-reinforced material. That is, about 13% and 20% higher than those found for an equivalent volume fraction of plain woven-reinforced composite.

For the case of biaxial NCF glass-reinforced polyester composites (33% volume fraction) the study is performed to investigate the performance of the composites vs. the woven roving reinforced composites. It was found from the fatigue strength tests, fatigue strength diagrams, and stiffness curves that model parameters concerning damage initiation, damage progression, coupling vectors, and passive damage parameters are identifiable. It was found that the composite had 13% greater ultimate tensile strength (UTS) than the composite that was woven roving reinforced due to enhanced fiber alignment and load distribution in the biaxial NCF structure. Another characteristic of the composite was a 20 % higher shear fatigue resistance in comparison to the woven roving reinforced composite, probably due to less fiber waviness and well transfer of stress load in the NCF laminate. The results obtained from these tests confirm that the biaxial NCF composites provide a better tensile and shear fatigue resistance compared to the woven roving composites in either case and, as such, could be deemed a preferred material choice for applications with high fatigue life and durability under cyclic loading.

Damage initiation under cyclic loading is calculated using critical normalized strain energy density, requiring one-stage tests on unidirectional reinforced composite pipe specimens to approximate ΔW(N) force-controlled tests, Table 3. A numerical DOE approach was implemented to systematically analyze the effect of fracture mode, angle, and stress conditions on critical normalized strain energy density. This allowed for structured parametric simulations without physical experiments.

Table 3. Numerical modeling setup for the determination of fracture mode-related critical normalized strain energy density

Fracture Mode	Angle	Characteristic Value Function
IFF1	90°	$\Delta W^{\perp\sigma}$
IFF2	90°	$\Delta W^{\perp\|\|}$
IFF3	90°	$\Delta W^{\perp\tau}$
FF1	0°	$\Delta W^{\|\|\sigma}$
FF2	0°	$\Delta W^{\|\|\tau}$

Due to the technologically related inaccessibility of an isolated i-UD base layer of GF-MLG/EP, reference values from the literature are used for damage initiation calculations. The fatigue strength values published for unidirectional glass fiber reinforced stronger epoxy resins in the fracture modes IFF1, IFF2, and IFF3 are converted into the critical normalized strain energy densities. This study uses IFF3 fracture mode to determine S-N curves for GF-MLG/EP composites under pressure pulsating load, revealing identical fatigue strength behavior and no stress redistribution in the textile composite (see Figure 5).

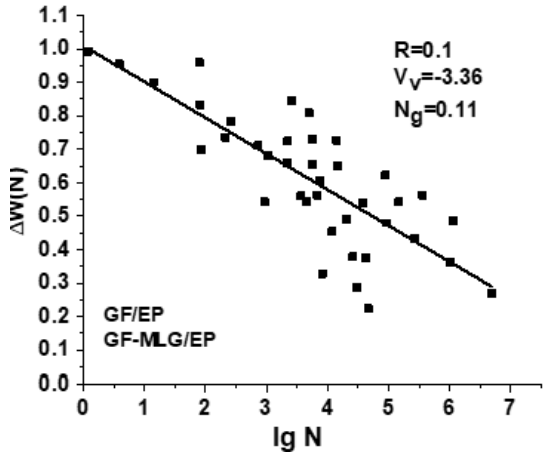

Figure 5. Normalized critical strain energy density for the i-UD base layer by GF-MLG/EP

The study presents a critical normalized shape change energy density for GF-MLG/EP for modeling damage initiation in fiber breakage modes.

$$\Delta W(N) = \left(\frac{1+3.36}{N+3.36}\right)^{0.11} \quad (15)$$

The service life of GF-MLG/EP can be calculated until damage initiation, but reliable data for fiber break modes FF 1 and FF 2 is lacking. High load amplitudes cause early damage initiation, allowing for accurate damage assumption.

Figure 6 shows a decrease in GF-MLG/EP stiffness and tensile pulsating stress, adjusting model parameters and determining the damage increment function. $\varphi^{||\sigma}$ based on the chosen mathematical formulation.

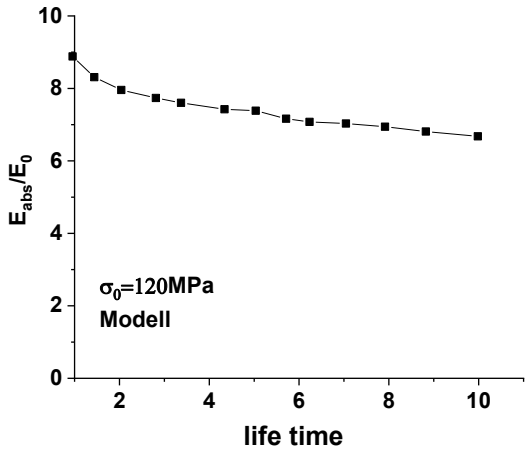

Figure 6. Study of determined decrease in stiffness of GF-MLG/EP and tensile pulsating stress

The model parameters are determined analogously by successive comparison with the experiment, as shown in Figure 6. A critical damage parameter Dc is chosen as the upper limit of the damage evolution decrease in rigidity.

The study calculates damage increase in the first and second phases of stiffness degradation, but the second phase cannot be modeled due to damage localization and end-of-life stability risk, only valid under pure shear stress state. Specific fatigue tests, like torsional vibration tests, are beneficial for assessing the increase in damage in fracture mode IFF2 on pipe specimens. In the literature to characterize the shear properties often used tension fatigue tests strip specimens with ±45° fiber orientation, on the other hand, are through on the layer plane characterized by a combined (σ2 and τ21) stress. The study reveals a superimposed damage evolution in fracture modes IFF1, IFF2, and FF1, which is not immediately apparent due to the associated fracture mode-related damage growth functions.

To determine the model parameters of the damage growth function $\varphi^{||\sigma}$ (fracture mode IFF2), the stiffness degradation with increasing torsional loading is used, see Figure 7.

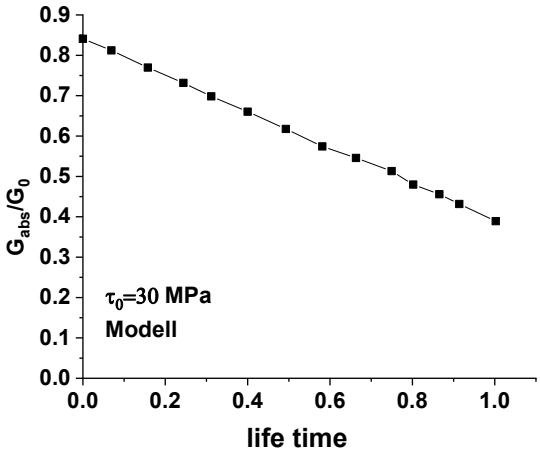

Figure 7. Study model approach and calculated stiffness degradation to determine the model parameters of $\varphi^{\perp\sigma}$

The growth functions for GF-MLG/EP composites selected according to the observed damage characteristics and those determined using the methods mentioned above and the associated model parameters are summarized in Table 4.

Table 4. Model parameters of the damage increment functions

Model	Model Parameter	Value
IFF1	c_1	7 E^{-5}
	D_s	4 E^{-1}
IFF2	c_2	8 E^{-18}
	c_3	12
	D_{c2}	40 E^{-2}
IFF1	c_4	6 E^{-10}
	c_5	18.46
	c_1	11 E^{-2}

The numerical results suggest that the model parameters c_4 and c_5 can be approximated as an increase in the CDS with a constant damage increase. The model only depicts damage initiation in fracture modes IFF3 and FF2, as no experimental increase in damage can be demonstrated.

The remaining components of the coupling vectors $q_6^{||\sigma}$, $q_6^{\perp\sigma}$ and $q_6^{\perp||}$, as well as the influencing parameters of the passive damage hi from the results of the tension-torsion and pressure-torsion fatigue tests on pipe specimens. The test results suggest that despite the micromechanically justified interaction of damage in failure mode FF 1 with the decrease in shear stiffness, there is no measurable coupling. This means that $q_6^{||\sigma} = 0$.

Table 5. Coupling parameters for GF-MLG/EP

Modeling Parameter	Value
$q_6^{\perp\sigma}$	1.8
$q_1^{\perp||}$	0.3
$q_2^{\perp||}$	0.5
h_i (I = 1.2)	0.5

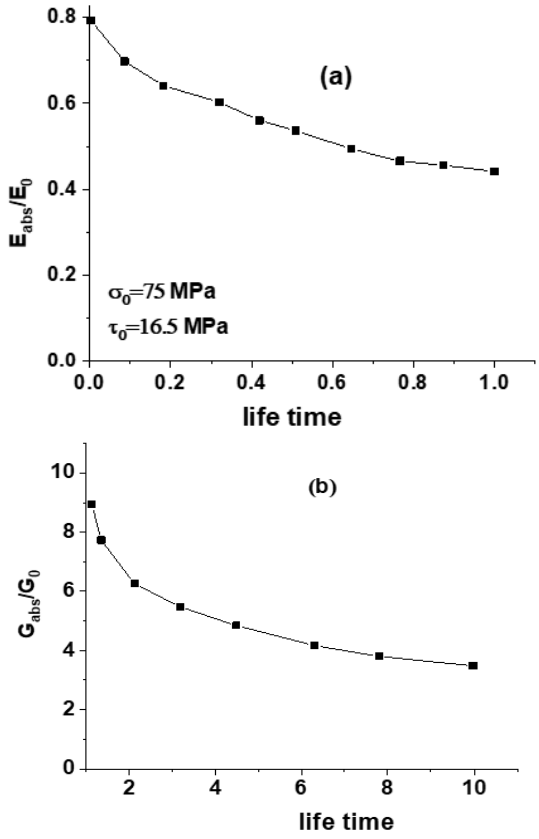

Figure 8. Identification of the coupling parameters based on the tensile stiffness (a) and decrease in shear stiffness (b) of GF-MLG/EP composites tensile, torsional load (LP2)

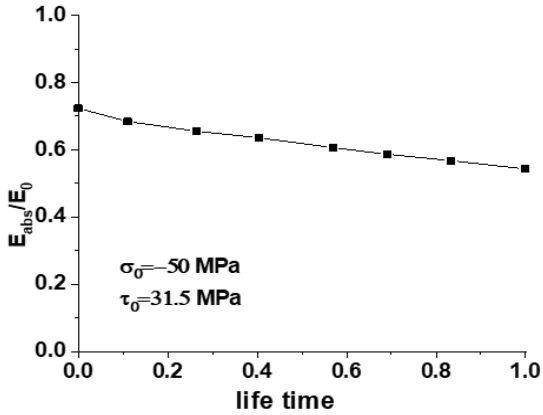

Figure 9. Numerical study to determine the drop in compressive stiffness with superimposed compressive shear stress

Conversely, damage in the IFF2 fracture mode influences the stiffness properties in the direction of the fibers with $q_1^{\perp||} \neq 0$. In addition, due to the almost identical damage phenomenology, coupling with the stiffness degradation in the 2-direction ($q_2^{\perp\sigma} \neq 0$) and vice versa ($q_6^{\perp\sigma} \neq 0$) was demonstrated. The parameter identification takes place with the iterative adaptation of the calculated numerical one, which determines the drop in rigidity under tensile torsional loading (see Figure 8). The resulting coupling parameters are given in Table 5.

The results of the pressure torsional fatigue tests are used to determine the influencing parameters of the passive damage, shown in Figure 9, which accorded with the numerical study cited in the literature.

4. CONCLUSIONS

This work developed a new degradation model for textile-reinforced plastics under cyclic loading using continuum-damage-mechanical approaches. The model involves an incremental calculation process considering damage initiation and evolution. The model decomposes the composite into a multilayer composite with idealized unidirectional base layers, and the direction-dependent damage evolution is calculated. This allows for the first modeling of successive failure behavior of textile composites under oscillating loads with tensile and shear components. Calibration of model parameters is determined through stress-strain hysteresis and fatigue strength diagrams.

This study presents a layer-by-layer lifetime modeling model that accurately predicts direction-dependent residual strength after cyclic loading. The model's practical performance is demonstrated in engineering practice, allowing efficient configuration determination for different material types. It also considers stress redistribution due to fracture mode-related and layered damage, enabling more realistic service life predictions. This knowledge contributes significantly to understanding textile-reinforced plastics' material behavior under cyclic loading.

Carbon fiber-reinforced composites had a tensile strength of 74.5 MPa, while glass fiber-reinforced composites (GF-MLG/EP) showed a significant reduction of stiffness, about 20%, more than linear stress, up to failure. In the degradation path of the textile-reinforced plastic composites, there were three stages of failure; aggressive, linear, and progressive stages.

However, mechanical properties were improved by 13% and 20% tensile strength and fatigue endurance, respectively, with NCF glass reinforced polyester material with 33 vol.% volume fraction relative to the equivalent volume fraction of woven roving reinforced composites in experiments. Important normalized strain energy density results on GF-MLG/EP are obtained as the IFF1 mode, IFF2 mode, IFF3 mode, FF1 mode and FF2 mode.

Initial phase damage initiation occurred at 25%-35%, structural stabilization at 10% -15%, and complete structural breakdown during the final phase. Four factors combined with the primary coupling factor and secondary coupling factor, as well as the shear influence factor and passive damage factor, govern the damage propagation in the material.

It was shown in the research that GF-MLG/EP has directional sensitivity for stiffness change from the fact that transverse cracks cause a 25% stiffness reduction through 10,000 cycles. For torsional conditions, the loading cycles reduce shear stiffness by 0.02%. The Biaxial NCF composites outperform woven fabric composites due to their superior properties with failure at 1,000,000 cycles in the stress levels of 30% - 40% of the UTS and resist fatigue damage.

Suggestions for future works could be considered to utilize the developed procedure to perform analysis on another type of matrices using different types of reinforcements.

REFERENCES

[1] Laghi, V., Palermo, M., Gasparini, G., Trombetti, T. (2020). Computational design and manufacturing of a half-scaled 3D-printed stainless steel diagrid column. Additive Manufacturing, 36: 101505. https://doi.org/10.1016/j.addma.2020.101505

[2] Li, Y., Feng, Z., Hao, L., Huang, L., Xin, C., Wang, Y., Bilotti, E., Essa, K., Zhang, H., Li, Z., Yan, F., Peijs, T. (2020). A review on functionally graded materials and structures via additive manufacturing: From multi-scale design to versatile functional properties. Advanced Materials Technologies, 5: 1900981. https://doi.org/10.1002/admt.201900981

[3] Vassilopoulos, A.P., Maier, J., Pinter, G., Gaier, C. (2020). Computational tools for the fatigue life modeling and prediction of composite materials and structures. In: Vassilopoulos A.P. (ed.) Fatigue life prediction of composites and composite structures (Second Edition), Woodhead Publishing. https://doi.org/10.1016/B978-0-08-102575-8.00018-8

[4] Kabir, S.M.F., Mathur, K., Seyam, A.F.M. (2020). A critical review on 3d printed continuous fiber-reinforced composites: History, mechanism, materials and properties. Composite Structures, 232: 111476. https://doi.org/10.1016/j.compstruct.2019.111476

[5] Dean, A., Kumar, A.V.P.K., Reinoso, J., Gerendt, C., Paggi, M., Mahdi, E., Rolfes, R. (2020). A multi-phase-field fracture model for long fiber reinforced composites based on the puck theory of failure. Composite Structures, 251: 112446. https://doi.org/10.1016/j.compstruct.2020.112446

[6] Tabrizi, I.E., Kefal, A., Zanjani, J.S.M., Akalin, C., Yildiz, M. (2019). Experimental and numerical investigation on fracture behavior of glass/carbon fiber hybrid composites using acoustic emission method and refined zigzag theory. Composite Structures, 223: 110971. https://doi.org/10.1016/j.compstruct.2019.110971

[7] Vassilopoulos, A.P. (2020). The history of fiber-reinforced polymer composite laminate fatigue. International Journal of Fatigue, 134: 105512. https://doi.org/10.1016/j.ijfatigue.2020.105512

[8] Kendall, K. (2020). Crack control: Using fracture theory to create tough new materials. Elsevier, Amsterdam. https://shop.elsevier.com/books/crack-control/kendall/978-0-12-821504-3.

[9] Tauber, J., Van Der Gucht, J., Dussi, S. (2022). Stretchy and disordered: Toward understanding fracture in soft network materials via mesoscopic computer simulations. The Journal of Chemical Physics, 156: 160901. https://doi.org/10.1063/5.0081316

[10] Lemcherreq, Y., Galkovski, T., Mata-Falcцën, J.,

Kaufmann, W. (2022). Application of distributed fibre optical sensing in reinforced concrete elements subjected to monotonic and cyclic loading. Sensors, 22: 2023. https://doi.org/10.3390/s22052023
[11] Dobrzański, L.A. (2021). Advanced composites with aluminum alloys matrix and their fabrication processes. In: Dobrzański L.A. (ed.) Advanced Aluminium Composites and Alloys. IntechOpen, Rijeka. https://doi.org/10.5772/intechopen.98677
[12] Yılmaz, N.D., Khan, A.G.M. (2019). Flexural behavior of textile-reinforced polymer composites. In: Jawaid M., Thariq M. & Saba N. (eds.) Mechanical and Physical Testing of Biocomposites, Fibre-Reinforced Composites and Hybrid Composites. Woodhead Publishing. https://doi.org/10.1016/B978-0-08-102292-4.00002-3
[13] Dönmez, D. (2021). Numerical study of behavior of textile-reinforced composite tubes under lateral compression. Mechanics Based Design of Structures and Machines, 51(7): 3738-3758. https://doi.org/10.1080/15397734.2021.1937214
[14] Mahdavi, H., Poulios, K., Niordson, C.F. (2020). Effect of superimposed compressive stresses on rolling contact fatigue initiation at hard and soft inclusions. International Journal of Fatigue, 134: 105399. https://doi.org/10.1016/j.ijfatigue.2019.105399
[15] Rizzo, F., Pinto, F., Meo, M. (2019). 3d Bio-inspired hierarchical discontinuous CFRP with enhanced ductility. Composite Structures, 226: 111202. https://doi.org/10.1016/j.compstruct.2019.111202
[16] Hamrat, M., Bouziadi, F., Boulekbache, B., Daouadji, T.H., Chergui, S., Labed A., Amziane, S. (2020). Experimental and numerical investigation on the deflection behavior of pre-cracked and repaired reinforced concrete beams with fiber-reinforced polymer. Construction and Building Materials, 249: 118745. https://doi.org/10.1016/j.conbuildmat.2020.118745
[17] Oz, F.E., Ahmadvashaghbash, S., Ersoy, N. (2019). Damage mode identification in transverse crack tension specimens using acoustic emission and correlation with finite element progressive damage model. Composites Part B: Engineering, 165: 84-95. https://doi.org/10.1016/j.compositesb.2018.11.104
[18] Gholipour, G., Zhang, C., Mousavi, A.A. (2020). Nonlinear numerical analysis and progressive damage assessment of a cable-stayed bridge pier subjected to ship collision. Marine Structures, 69: 102662. https://doi.org/10.1016/j.marstruc.2019.102662
[19] Rezasefat, M., Gonzalez-Jimenez, A., Giglio, M., Manes, A. (2021). An evaluation of cuntze and puck inter fibre failure criteria in simulation of thin cfrp plates subjected to low velocity impact. Composite Structures, 278: 114654. https://doi.org/10.1016/j.compstruct.2021.114654
[20] Zhang, C., Huang, Y., Tao, C., Qiu, J., Ji, H. (2022). Fatigue property evaluation for fiber reinforced plastics based on mode conversion effect of guided wave. Composites Science and Technology, 223: 109405. https://doi.org/10.1016/j.compscitech.2022.109405
[21] Thomason, J.L. (2019). Glass fibre sizing: A review. Composites Part A: Applied Science and Manufacturing, 127: 105619. https://doi.org/10.1016/j.compositesa.2019.105619
[22] Hassani, F.Z.S.A., Bouhfid, R., Qaiss, A. (2021). Modeling of damage evaluation and failure of laminated composite materials. In: Jawaid M., Hamdan A., Hameed Sultan M.T. (eds.) Structural Health Monitoring System for Synthetic. Hybrid and Natural Fiber Composites, Springer Singapore, Singapore. https://doi.org/10.1007/978-981-15-8840-2_8
[23] Su, X., Yin, S., Yang, Y., Feng, J., Li, L. (2022). Comparative analysis of flexural performance of old full-scale hollow slab beams reinforced with fiber composites. Construction and Building Materials, 338: 127657. https://doi.org/10.1016/j.conbuildmat.2022.127657
[24] Adam, V., Bielak, J., Dommes, C., Will, N., Hegger, J. (2020). Flexural and shear tests on reinforced concrete bridge deck slab segments with a textile-reinforced concrete strengthening layer. Materials, 13: 4210. https://doi.org/10.3390/ma13184210
[25] Ferdous, W., Manalo, A., Peauril, J., Salih, C., Reddy, K.R., Yu, P., Schubel, P., Heyer T. (2020). Testing and modelling the fatigue behaviour of GFRP composites–effect of stress level, stress concentration and frequency. Engineering Science and Technology, an International Journal, 23: 1223-1232. https://doi.org/10.1016/j.jestch.2020.01.001

NOMENCLATURE

Symbol/ Abbreviation	Definition	Unit
c_1, c_2, c_3	Model parameters for damage evolution functions	-
c_4, c_5	Secondary damage coefficient	-
D	Damage parameter	-
Dc2	Model parameter for certain types of stress redistribution	-
Dc	Critical damage (used in load progression equations)	-
Ds	Saturation Limit (used in damage models)	-
F	Material stress	MPa
FF1, FF2	Fiber fracture failure modes	-
hi	Influence parameter related to passive damage	-
IFF1, IFF2, IFF3	Inter-fiber failure modes for 90° and 0° fiber orientations	-
Nc	Number of cycles	-
q	Coupling factor between different damage modes	-
R	Cyclic loading	-
V_f	Fiber volume fraction	%
$\varphi(phi)^*$	Damage growth function	-
Edyn(N)	Dynamic modulus as functions of cycle number N	MPa
Gdyn(N)	Shear modulus as functions of cycle number N	MPa
GF-MLG/EP	Glass fiber - multi-layered glass/ epoxy resin composite	-
UTS	Ultimate tensile strength	MPa